First Study on Phosphonite-Coordinated Ruthenium Sensitizers for Efficient Photocatalytic Hydrogen Evolution

T. Swetha,[†,‡,#] Indranil Mondal,[‡,§,#] K. Bhanuprakash,[†,‡] Ujjwal Pal,*[,‡,§] and Surya Prakash Singh*[,†,‡]

[†]Inorganic and Physical Chemistry Division, CSIR-Indian Institute of Chemical Technology, Uppal road, Tarnaka, Hyderabad-500007, India

[‡]Network Institute of Solar Energy, (CSIR-NISE) and Academy of Scientific and Innovative Research (AcSIR), New Delhi-110001, India

[§]Department of Chemistry and Biomimetics, CSIR-Central Mechanical Engineering Research Institute, M.G Avenue, Durgapur-713209, West Bengal India

Ⓢ *Supporting Information*

ABSTRACT: For the first time we report the design and syntheses of phosphonite coordinated ruthenium(II) sensitizers bearing ĈN̂N ligand and/or terpyridine derivatives carboxylate anchor (**GS11**, **GS12**. and **GS13**) and its application for hydrogen production over Pt–TiO$_2$ system. These heteroleptic complexes exhibit broad metal-to-ligand charge transfer transition band over the whole visible regime extending up to 900 nm. DFT calculations of these complexes show that the HOMO is distributed over the Ru and Cl atom whereas; LUMO is localized on the polypyridile ligand, which are anchored on TiO$_2$ surface. Among the sensitizers tested for photocatalytic hydrogen evolution, **GS12** exhibited a maximum turnover number (TON) 8605 (for 8h), which is very high compared to the reference sensitizer (N719) with TON 163 under similar evaluation condition. The dependence of the hydrogen evolution rate at different pH using **GS11**, **GS12**, **GS13**, and DX-1-sensitized Pt–TiO$_2$ has been studied and the maximum H$_2$ production yield was obtained at pH 7 for all sensitizers.

KEYWORDS: *phosphonite-coordinated ruthenium(II) sensitizers, carboxylate anchor, hydrogen evolution, DFT studies, high TON*
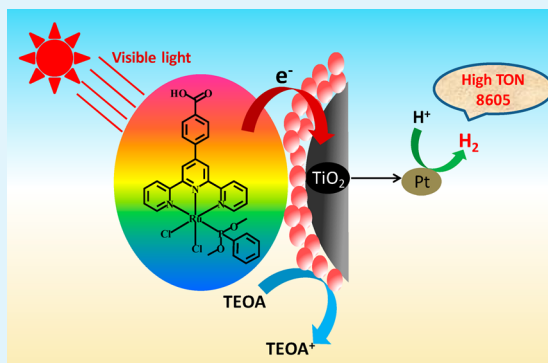
1. INTRODUCTION

The establishment of the low-carbon society for green globalization requires an effective conversion of renewable energy to clean fuel source and hydrogen production using solar energy can be the quintessential choice to serve this purpose.[1] Among all the methods discovered so far, photocatalytic hydrogen production using semiconductor is considered as one of the promising approach for conversion of solar to chemical energy. Since the water splitting effect using TiO$_2$ and a Pt black system was reported in 1972 by Honda–Fujishima,[2] photocatalytic hydrogen evolution from water sacrificial electron donor (SED) mixture has been widely investigated with TiO$_2$[3] and other semiconductors.[4] However, the wide band gap of these semiconductor is the main drawback as visible-light-driven photocatalyst requires a band gap of less than 3.0 eV ($\lambda > 415$ nm). To date, dye sensitization of the semiconductors has been chosen as an alternative approach to achieve hydrogen production under visible light. Although there has been some remarkable progress in the design and development of dyes, yet there should definitely be more extensive studies and clear understanding about sensitizers for fabricating more active systems.

As of now, Ru,[5] Pt,[6] and Ni complexes,[7] metalloporphyrins,[5] and phthalocyanines[8] have been successfully employed as the

inorganic sensitizers for visible-light induced hydrogen production from water. In particular, as visible light sensitizers on TiO$_2$, ruthenium-based dyes have been extensively studied toward photocatalytic H$_2$ evolution for their typically long electronic excited state lifetime. In contrast, a dimer of ruthenium complex Ru$_2$(bpy)$_4$(BL) (ClO$_4$)$_2$ (bpy = bipyridyl, BL = bridging ligand) showed unique "antenna effect" to capture more visible light for remarkable hydrogen production over Pt/dye/TiO$_2$ system.[9] However, tuning of the spectral properties to improve the light harvesting capability of these complexes is still an utterly challenging topic for the researchers.

In recent years, panchromatic sensitization by heteroleptic Ru complexes is under intensive research focus in the application of dye-sensitized solar cell.[10] Especially thiocyanate based ruthenium complexes are well-known for showing panchromatic light harvesting nature.[10] with this regards, Meyer et al. has established a good correlation between the enhanced light harvesting capability and ligand characteristics.[11] Introduction of a ligand with low lying π^* molecular orbital and strong donor ability
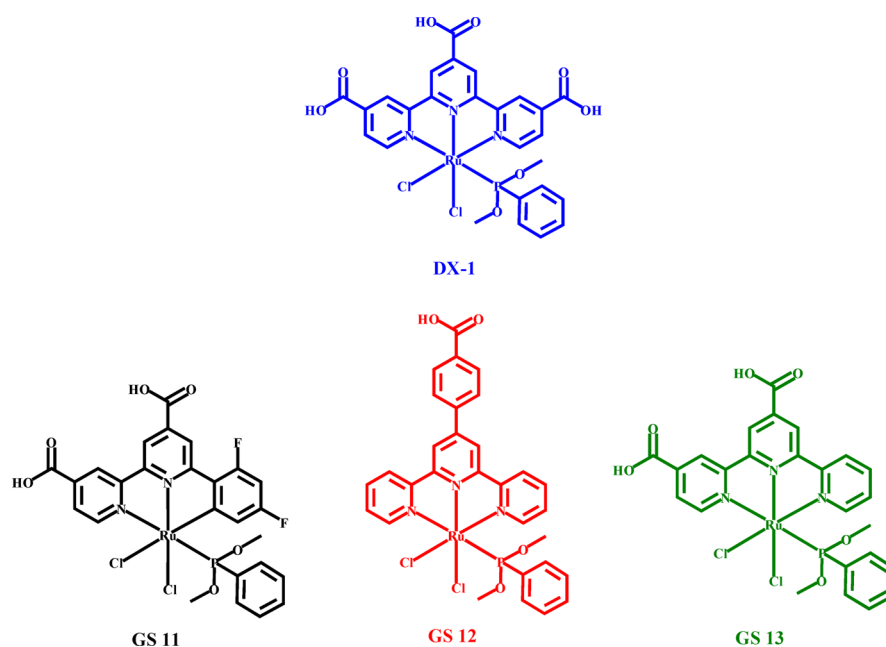
Figure 1. Molecular structures of DX-1 (Reproduced with permission from ref 12. Copyright 2013, Nature Publishing Group), **GS11**, **GS12**, and **GS13** sensitizers.

extends the absorption toward more visible region which turned into a basic principle for panchromatic light harvesting nature of sensitizers. It is noteworthy that, Kinoshita et al. has developed first time a phosphonite-coordinated Ru complex for wideband dye sensitized solar cells.[12] However, as far as we aware, the application of phosphonite coordinated Ru complex and its panchromatic sensitization in photocatalytic H_2 evolution has not been done before.

We herein report highly efficient, visible-light-induced photocatalytic hydrogen production over newly synthesized phosphonite coordinated ruthenium sensitizers (**GS11**, **GS12**, and **GS13**, Figure 1) and state-of-art dye DX-1-sensitized Pt−TiO_2 system under solar simulated light intensity of ∼2 sun. We found that these heteroleptic complexes containing a tridentate ligand together with chloride and phosphonite based ligand showing interesting panchromatic sensitization for solar assisted proton reduction form water SED mixture. It can also be envisioned that employing different ancillary has a significant effect on the tuning of sensitizer's LUMO level, which turn out to be a controlling factor for the electron injection from dye to conduction band (CB) of TiO_2. Density functional theory (DFT) calculations were carried out for **GS11** to **GS13** to understand their structural, electronic, and photophysical properties.

2. RESULTS AND DISCUSSION

2.1. Synthesis of GS11, GS12, and GS13. The stepwise synthesis protocol of the ligands and sensitizers has been illustrated in the Scheme 1, experimental approaches and the characterization details (Figure S1 and Figure S2) have been discussed in Supporting Information. Dimethyl-6-chloro-2,2′-bipyridine-4,4′-dicarboxylate 3 was prepared by the oxidation reaction of 4,4′- bis(methoxycarbonyl)-2,2′-bipyridine with meta-chloroperbenzoic acid (MCPBA), followed by chlorination of 2 with $POCl_3$. The Suzuki coupling reaction of 3 with 2,4-difluorophenylboronic acid yielded 4. The hydrolysis reaction of 4 with aqueous KOH was converted to the ĈNN ligand L1.[13] Similarly, L2 was synthesized using Suzuki coupling reaction[14−16] of 2-(4-chloro-6-(pyridin-2-yl) pyridin-2-yl)

pyridine 5 with aryl boronic acid followed by the hydrolysis in the presence of aqueous KOH. The L3 was prepared by the hydrolysis of commercially available diethyl [2,2′,6′, 2″-terpyridine]-4,4′-dicarboxylate (8) under basic conditions.[17] Each terpyridine based ligand was obtained in moderate yield (54−62%). The final step was performed by the addition of ancillary ligands L1, L2, and L3 to $RuCl_3 \cdot 3H_2O$ (ruthenium trichloride trihydrate) and refluxed for 4 h in CH_3OH. Thereafter one chloro ligand was substituted by phosphonite ligand using Et_3N in DMF medium at 70 °C, followed by the addition of CF_3COOH to afford corresponding sensitizers in good yields.

2.2. Optical Properties. Absorption spectra of these sensitizers were recorded in DMF solution (Figure 2a) and corresponding details were appended in Table 1. The UV−vis spectra in of region 250−900 nm was recorded where different characteristic absorption pattern was observed for DX-1, **GS11**, **GS12**, and **GS13** sensitizers with varying molar extinction coefficient. These sensitizers exhibited absorption in higher energy region at around 320 nm, which can be attributed to the $\pi-\pi^*$ transition of ancillary ligand. The low energy absorption band in the 500−900 nm region are assigned to MLCT bands transitions, which are characteristic of ruthenium polypyridyl sensitizers.[18] The MLCT band of **GS11** and **GS13** at around 600 nm is higher in intensity than the MLCT band of DX-1. In particular, this band for DX-1 showed a bathochromic shift in comparison to **GS12** and **GS13**, which may attributes to the increasing order of the stabilization of LUMO level due to increase in the number of electron withdrawing carboxylic groups.[19] In addition, **GS13** exhibited higher-intensity and broad electronic absorption peak at longer wavelength (800 nm) in comparison to DX-1, may attributed to near-infrared, spin-forbidden singlet-to-triplet direct transitions in a phosphonite-coordinated Ru(II) sensitizer. The molar extinction coefficients of **GS11**, **GS12**, **GS13**, and DX-1 are 6872, 528, 2469, and 2104 M^- cm^- at 583, 533, 797, and 791 nm, respectively. The sensitizer **GS12** showed lower molar extinction coefficient compared to **GS11**, **GS13**, and DX-1. This may be attributed due to the twisted nature of phenyl moiety on central pyridine ring of

Scheme 1. Synthesis of GS11, GS12, and GS13 Sensitizers[A]
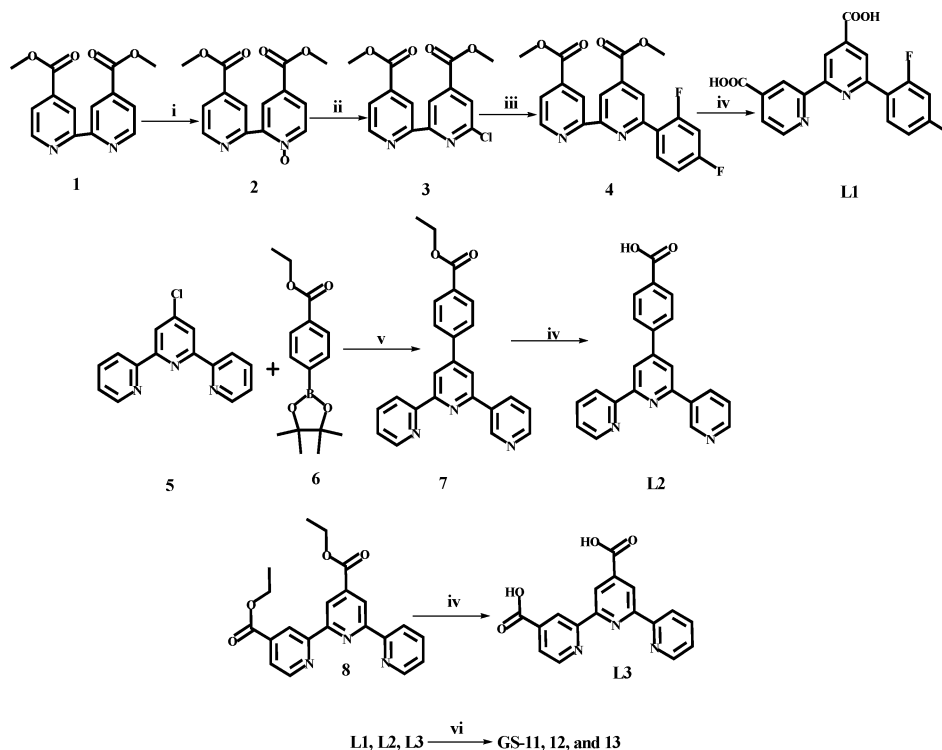
[A]Reagents and conditions: (i) MCPBA, CH_2Cl_2; (ii) $POCl_3$; (iii) 2,4 difluorophenylboronic acid, $Pd(PPh_3)_4$, Na_2CO_3, THF, 80 °C, 6 h; (iv) KOH, MeOH, H_2O, 70 °C, 6 h; (v) $Pd(PPh_3)_4$, Na_2CO_3, THF, 80 °C, 16 h; (vi) $RuCl_3 \cdot 3H_2O$, dehydrated ethanol, 70 °C, 6 h, phenyl dimethoxyphosphine, NEt_3, TFA, 70 °C.
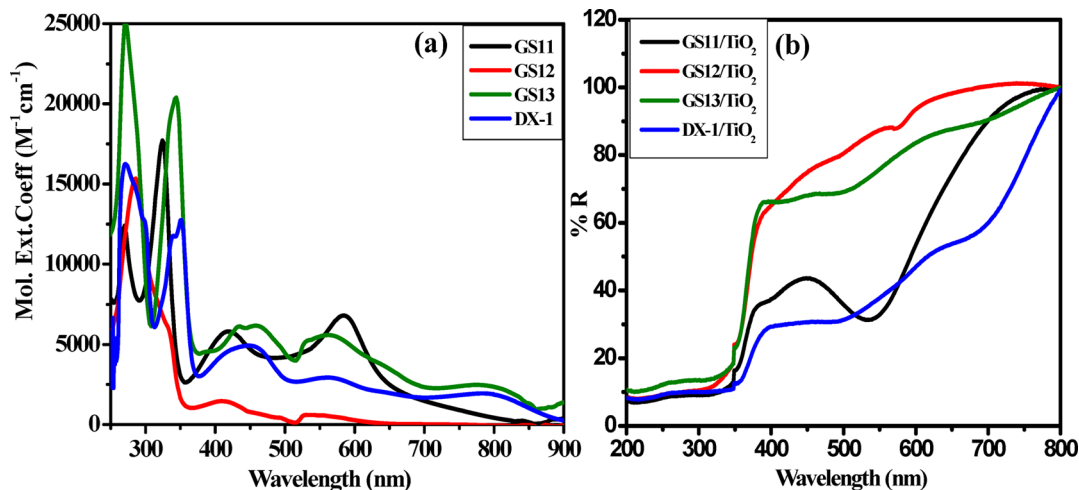

Figure 2. (a) Absorption spectra of **GS11**, **GS12**, **GS13**, and DX-1 in MeOH. (b) DRS of different Dye/TiO_2 composites.

terpyridine ligand.[20] Electronic absorption and emission intersection spectra of **GS11**, **GS12**, and **GS13** are depicted in (Figure S3, Supporting Information).

Prominent visible to NIR emission was observed for GS sensitizers, as **GS11** and **GS12** showed emission maxima at 638 and 652 nm, respectively, whereas emission maxima of **GS13** appeared at 842 nm. In this approach, sensitizer's concentration is of less than 10^{-5} M was utilized to avoid intermolecular H-bonding through carboxylic groups and/or $\pi-\pi^*$ stacking between ancillary fragments.

To enquire the optical properties of metal complex sensitizers after being surface attached onto TiO_2, diffuse reflectance spectroscopy (DRS) was carried out for all dye/TiO_2 composites, where the spectra have been recorded in the reflectance mode. As shown in the Figure 2b, optical properties of the dye/TiO_2 composites fully complement the optical features of individual sensitizers. The extended long tail toward far-visible region for **GS11** is prominent in the spectra of **GS11**/TiO_2 composite. After being sensitized on TiO_2 surface, the characteristic absorption bands for **GS11**, **GS13**, and **DX-1** appeared at lower wavelength in comparison to solution phase spectra of pure sensitizers. This could be assigned as aggregation of dyes on to TiO_2. Whereas, there is no such shifting of band was observed for **GS12**, could be ascribed to proper formation of esteric linkage and low

Table 1. Optical Parameters of Sensitizer GS11, GS12, GS13, and DX-1

dye	λ_{max} (ε) (M^{-1} cm^{-1}) [nm][a]	λ_{em}[b] (nm)	E_{oxd} [V][c]	E_{0-0} [eV][d]	LUMO [V][c]
GS11	583 (6872)	748	0.147	1.962	−1.815
GS12	533 (528)	733	0.216	2.066	−1.850
GS13	797 (2469)	831	0.212	1.585	−1.373
DX-1	791 (2014)	∼950	0.228	1.610	−1.382

[a]Absorption spectra was recorded in DMF solutions at 298 K. [b]Emission spectra was recorded in DMF solutions at 298 K. [c]Redox potentials were measured by DPV in DMF vs ferrocene/ferrocenium (Fc/Fc$^+$) with 0.1 M n-Bu$_4$NPF$_6$ as supporting electrolyte (scanning rate = 100 mV s, working electrode and counter electrode = Pt rod and Pt wire, and reference electrode = Ag/Agcl). The HOMO and LUMO were calculated with the following formulas: HOMO = E_{oxi} − $E_{Fc/Fc+}$ V; LUMO = HOMO − E_{0-0}. [d]The band gap, E_{0-0}, was derived from the intersection of the absorption and emission spectra.

aggregation of dye on TiO$_2$ surface which is also found to be common for N719 dye.[21] It is also worth mentioning that all dye/TiO$_2$ composite and TiO$_2$ shows characteristic absorption band around 380 nm because of its fundamental absorption of Ti−O bond in ultraviolet light range.

2.3. Electrochemical Studies. To investigate the electrochemical properties of the Ru sensitizers and to evaluate the possibility of electron injection from excited sensitizer to the conduction band (CB) of TiO$_2$, Differential Pulse Voltammetry (DPV) were performed with 0.1 M tetrabutylammonium hexafluorophosphate as supporting electrolyte in DMF solution (Figure 3a). All potentials were internally referenced to the ferrocene/ferrocenium (Fc/Fc+) couple which has the redox potential of ($E_{Fc/Fc+}$) 0.510 V vs Ag/AgCl. The first oxidation potential of the dyes have also been determined form their corresponding peak potential and incorporated in the Table 1. The LUMO energy values of **GS11**, **GS12**, **GS13**, and DX-1 are 1.815, −1.850, −1.373, and −1.382 V vs (Fc$^+$/Fc) respectively. The ancillary ligand (CN̂N ligand) in **GS11** is little different from other three dyes. Hence, in all cases the oxidation potentials of the LUMO level is sufficiently negative for energetically favorable solar illuminated excited state electron injection, while considering the conduction band alignment of the TiO$_2$.[22] The schematic energy levels of **GS11**, **GS12**, **GS13**, and DX-1 based on absorption and electrochemical data shown in Figure 3b.

2.4. Absorption Kinetics Studies. We have investigated the adsorption kinetics of phosphine coordinated Ru-sensitizers on

TiO$_2$ surface using 8 × 10^{-2} mM dye solutions and 10 mg of TiO$_2$, and the results were depicted in Figure 4. Typically, in photocatalytic proton reduction from water using dye loaded powder photocatalyst, amount of dye adsorbed on to the surface of TiO$_2$ semiconductor particle is estimated spectrophotometrically by measuring the difference in absorbance of free dye in aqueous solution with that of the supernatant liquid obtained after filtration/centrifugation. Here, the amount of adsorbed dye (equilibrium dye loading) on powder TiO$_2$ surface was measured as a function of suspension (adsorption) time. We can get a closer idea on the rate of the absorption of each dye onto TiO$_2$ surface by fitting the data on a first order exponential decay equation as mentioned below.

$$\text{Abs}(t) = \text{Abs}(eq) + Ae^{-(kt)}$$

Here, Abs(t) is the absorbance of the unabsorbed dye at particular time t, Abs(eq) is absorbance of the unabsorbed dye at equilibrium loading condition, A is fitting constan,t and k (min^{-1}) is rate constant for binding kinetics in terms of unabsorbed dye that remain in the solution. The greater k value signifies the slower rate of dye absorption and vice verse. As shown in Figure 4, the calculated k values are in good accordance with the anchoring group present in dye molecule. The lowest k value of 25.62 min^{-1} is attributable to the slow absorption of **GS12** which has one anchoring group. Thus, we speculate that, little bulky ancillary in **GS12** may block the recombination between the photoinjected electrons in the titanium and the oxidized SED species. The similar phenomena have been reported by Durant and co-workers in dye sensitized solar cell application.[23] Furthermore, we have also estimated the equilibrium loading of the sensitizers for 10 mg of TiO$_2$ which were 0.57, 0.37, 0.12, and 0.3 μmol for **GS11**, **GS12**, **GS13**, and DX-1, respectively. The low equilibrium loading of **GS13** could be the reason for lower hydrogen production activity.

2.4. Photocatalytic Hydrogen Generation. To assess the performance of these dyes for photocatalytic proton reduction from water SED mixture, the photocatalytic experiment of dye/Pt−TiO$_2$ systems containing dyes (**GS11**−**GS13** and DX-1) was investigated in 20 mL of 10 vol % aqueous triethanolamine (TEOA). All Dye/Pt-TiO$_2$ catalysts were fabricated on commercially available TiO$_2$ anatase particles by Pt photodeposition in methanol using a Xe lamp (450 W).[24] After this photodeposition, the dye was loaded onto the Pt-TiO$_2$ particles by solution processing in the presence of dye solution in methanol at
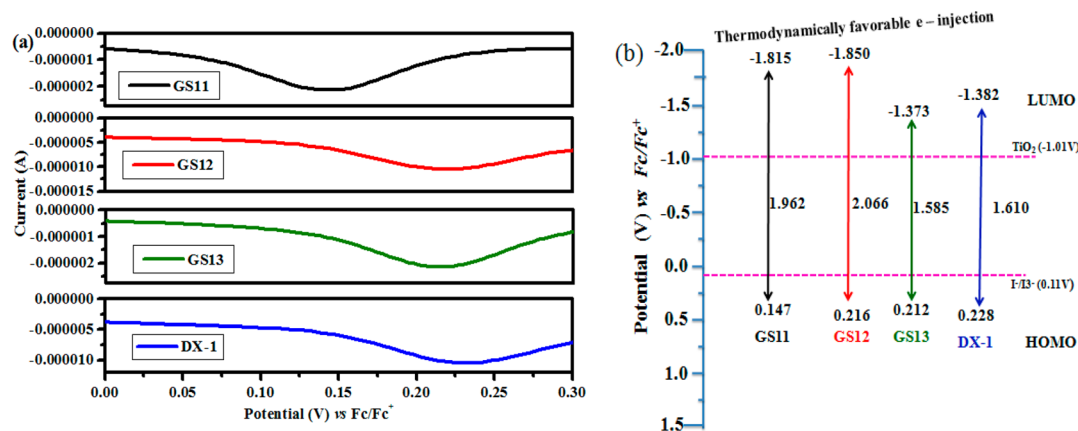

Figure 3. (a) Differential pulse voltammograms of **GS11**, **GS12**, **GS13**, and DX-1. (b) The schematic energy levels of **GS11**, **GS12**, **GS13**, and DX-1 based on absorption and electrochemical data.
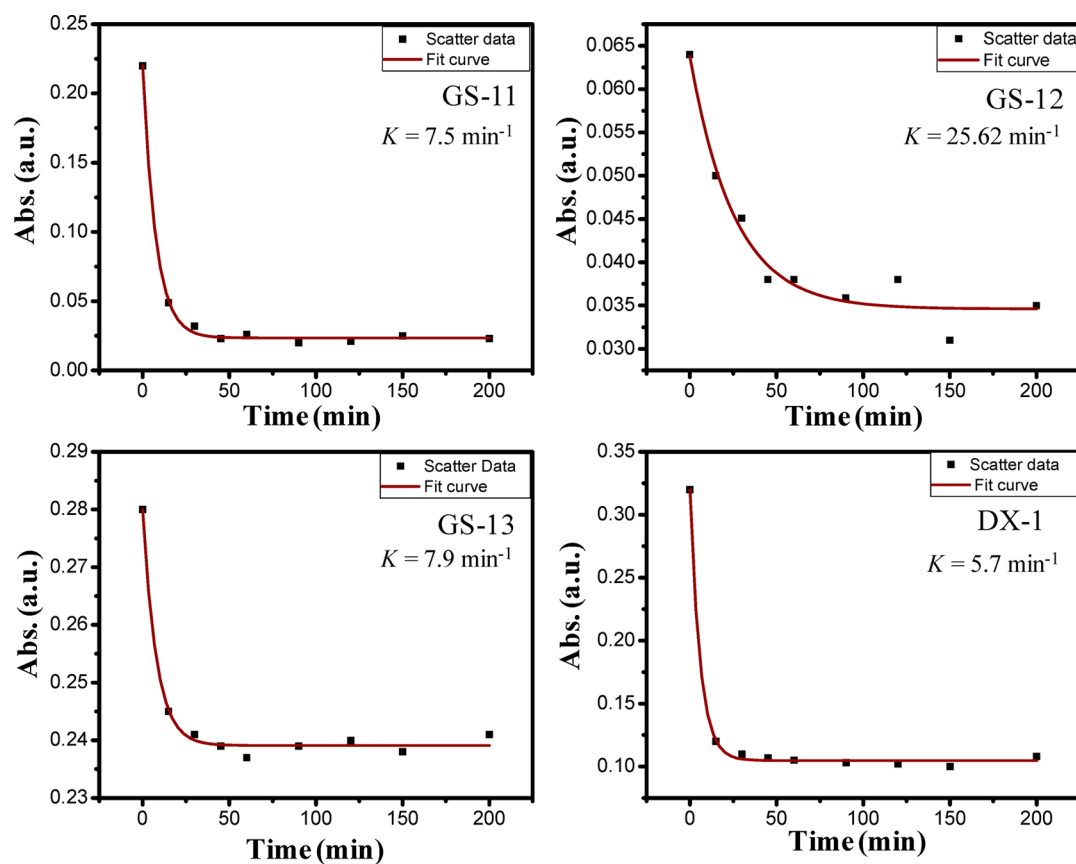
Figure 4. Absorption measured for different Ru-sensitizers at concentration 8×10^{-2} mM in the presence of 10 mg TiO_2 at room temperature.
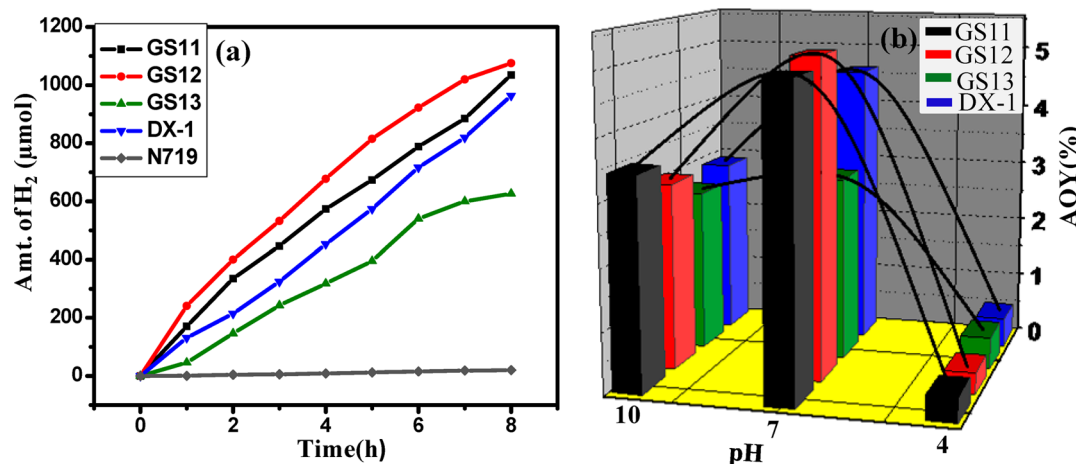

Figure 5. (a) Time courses of photocatalytic H_2 evolution over different dye/Pt−TiO_2 composite and (b) apparent quantum yield (AQY %) of H_2 generation at different pH. Reaction condition: 10% v/v TEOA, 400 W medium pressure Hg vapor lamp as light source, room temperature, dye concentration is 0.25 μmol/10 mg catalyst.

room temperature for 12 h. The reflectance absorption spectra of the TiO_2 particles showed peaks at the same wavelengths as for dye/TiO_2 composite, confirming the appropriate loading of the dyes.

The obvious effect of the sensitizers for photocatalytic H_2 production is shown in Figure S4 (Supporting Information) as **GS12** dye sensitized photocatalyst showed high H_2 production yield in comparison to bare and platinized TiO_2 under similar experimental condition. Figure 5a shows temporal plots for the H_2 generation using the catalysts of 0.25 μmol dye/10 mg Pt−TiO_2. One wt % Pt was used as the cocatalyst in all photocatalyst

composites as presumably excess Pt loading would lead to more extensive quenching of excited state dye molecules. Moreover, larger Pt particles may be responsible for the band gap narrowing of semiconductor which increases the electron hole recombination.[25,26] As shown in Figure 5b, **GS12** exhibits the greater efficiency with H_2 generation yield ∼1.1 mmol though it has only one electron withdrawing carboxylic anchoring group. This result may due to the more negative energy of the LUMO level in **GS12**, promotes easy electron transfer from dye to CB of TiO_2. Moreover, as confirmed by the DRS analysis, low dye aggregation of **GS12** on TiO_2 surface may also facilitate the effective electron

Table 2. Solar Driven H$_2$ Production over Different Dye/Pt−TiO$_2$

dye	TON[a]	%AQY[b]
GS11	8277	4.96
GS12	8605	5.16
GS13	5010	3
DX-1	7711	4.62
N719	163	0.95

[a]Turn over number was calculated after 8 h using, TON = (2 × amount of H$_2$)/amount of sensitizer}. [b]Apparent quantum yield (AQY%) = {(2 × number of evolved H$_2$ molecule)/number of incident photon}.

injection form dye to TiO$_2$. On the other hand, the H$_2$ production yield of DX-1 reached up to TON 7711 which is 2700 more in comparison to **GS13** after 8 h irradiation, (Table 2) which might be attributable to the greater number of carboxylic group in DX-1, accelerates the electron transfer at the dye/TiO$_2$ interface more prominently. Thus, it is worth mentioning here that besides the energy of LUMO level, electron injection from dye to TiO$_2$ is also depends on the carboxylic group, which is beneficial for both dye absorption and formation of electron transfer path.[27−30]

Notably, **GS11** exhibited better photoactivity with 4.96 AQY in comparison to **GS13** and DX-1, which may ascribed to stabilization of LUMO level by two fluorine atoms.

The pH value often has a significant effect on photocatalytic reaction, especially for dye-sensitized photocatalysts in the presence of a sacrificial agent. This is because it will influence the existing state of the dye, electron donor reagent and esteric bond that forms in between dye and TiO$_2$.[31,32] The effect of pH has been screened with all dye/Pt−TiO$_2$ in aqueous TEOA medium where the pH was adjusted by addition of 1(M) HCl (Figure 5b). The rate of H$_2$ production was decreased immensely at pH 4 for all photocatalysts. This is because in acidic medium protonation of the surface titanol groups inhibited the formation of, esteric linkage effectively.[33] The effect of pH on H$_2$ production has followed quite similar trend for all catalysts as at neutral medium the photocatalysts are giving the maximum efficiency which immediately fall down when pH was maintained at 10. At higher pH, the carboxyl groups of sensitizers were deprotonated, so the dye could not adsorb on TiO$_2$ surface effectively because of electrostatic repulsion force. Moreover, the pH values can also regulate the existing state of the sacrificial agent. TEOA was protonated in acidic solution, so its ability of donating electrons would weaken, which might influence the regeneration of oxidized dye molecules It is well-known that in aqueous solutions, the band edges of TiO$_2$ display a Nernstian dependence with the solution pH, moving ~60 mV per pH unit due to surface protonation/deprotonation.[34] This could be a reason for change in the thermodynamic driving force for charge injection from dye to TiO$_2$ conduction band. In a dye-sensitized system, dye desorption under long-term stirring under aqueous conditions is inevitable.[9] Moreover, during the irradiation process, many photogenerated species may be produced along with the decomposition of TEOA, may play a detrimental role in hydrogen production.[9]

Stability of the sensitizers was examined over 24 h. All the sensitizers exhibited good stability for hydrogen production under prolongs irradiation, as reduced catalytic activity was observed at third cycle (Figure 6). The lowering of photoactivity may due to partial dissolution of dye and consumption of sacrificial electron donor.
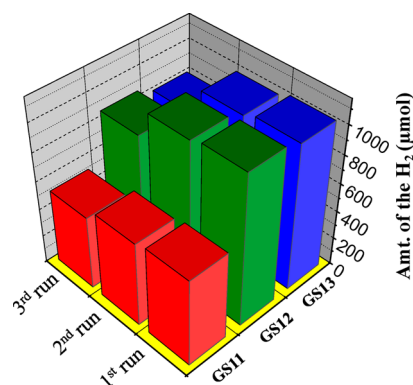

Figure 6. Histogram for reproducibility of photocatalytic H$_2$ production over different dye/Pt−TiO$_2$ composites. After each run, the reaction vessel was evacuated in the dark condition. Reaction condition: 10% v/v TEOA, 400 W medium pressure Hg vapor lamp as light source, room temperature, dye concentration is 0.25 μmol/10 mg catalyst.

3. THEORETICAL STUDIES (DFT CALCULATION)

The location of the HOMO−LUMO and the electronic properties of the **GS11**, **GS12**, and **GS13** dyes were theoretically investigated by using DFT in gas phase (Figures S5−S7) shows the isodensity surface contours of HOMO, HOMO−1, HOMO−2, HOMO−3, LUMO, LUMO+1, LUMO+2 and LUMO+3 for the sensitizers. The percentage of the frontier molecular orbitals contribution is shown in the Supporting Information. The HOMO of the **GS11**, **GS12**, and **GS13** are mainly populated over the ruthenium metal with significant contribution from Cl atom. On the contrary, LUMO of dyes are predominantly localized over polypyridyl. HOMO, HOMO−1, and HOMO−2 orbital sensitizers have predominant ruthenium t2g character. On the other hand, the orbital contributions toward the LUMO of the as-prepared sensitizers are quite similar to each other because the LUMO results mainly from the orbital delocalization of the polypyridyl moieties of the ancillary ligands. On photoexcitation, electron density moves from Ru−Cl unit to the polypyridyl moiety. Accordingly, the photoinduced electron transfer from dye to TiO$_2$ nanoparticle can efficiently occur at the HOMO−LUMO excitation. The HOMO and LUMO energies of the sensitizers evaluated theoretically are incorporated in Table S1 (Supporting Information).

On the basis of the optical, electrochemical and theoretical characterization, the conceptual mechanism for photocatalytic hydrogen evolution has been diagrammatically represented in Figure 7. The major electron density of HOMO is mainly
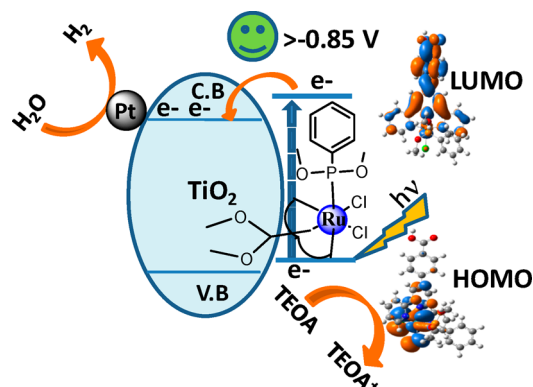

Figure 7. Graphical representation of dye sensitized photocatalytic hydrogen production.

delocalized on Ru−Cl units, which upon photoirradiation, rapidly inject electron into LUMO (majorly located on the ancillary ligand) of the dye. It is indeed the esteric linkage between dye and TiO$_2$, which acts as the electron transfer path. Subsequently, electrons reduce the water molecule at the Pt center. It can be speculated that these sensitizers may possesses a same order of emission lifetime with that of reported DX-1.[12] Eventually, it is still sufficient for electron injection into the conduction band (CB) of the TiO$_2$ nanoparticle because, injection from the ^{3}MLCT state to the TiO$_2$ conduction band occurs on a time scale of ∼10−100 ps.[12] The regeneration of the oxidized dye species takes place in a consecutive manner when SED donates electron into the HOMO level of the oxidized dye species (HOMO−1).

4. CONCLUSION

For the first time, we have successfully demonstrated the highly efficient panchromatic dye-sensitized photocatalytic hydrogen production over dye/Pt−TiO$_2$ composite in aqueous triethanolamine medium under visible light irradiation. The newly designed and synthesized phosphonite coordinated ruthenium sensitizers show pronounced light harvesting capability up to near IR region. The calculated LUMO energy values for sensitizers ensure the favorable electron injection from dye to TiO$_2$ nanoparticle. A very remarkable hydrogen production yield was obtained with TON 8605 for **GS12** after 8 h, which was almost 52 times higher than the reference dye N719 in our experimental condition. These encouraging finding insist us to synthesize more derivatives of phosphonite coordinated ruthenium complexes to get more high photoactivity.

5. EXPERIMENTAL SECTION

5.1. Photocatalytic Experiment. The photocatalytic hydrogen generation experiments were carried out in a 100 mL Pyrex glass reactor with flat optical entry window and external cooling jacket. Twenty milliliters of aqueous suspension containing 10 mg of photocatalysts and 10 vol % of SED was taken as the reaction mixture. The reactor was sealed with silicon septum and kept under ultrasonic treatment for 2 min to suspend the catalyst completely in the water/SED system. Before light irradiation dissolved oxygen was removed by 20 min evacuation followed by bubbling of argon gas for 30 min. As an external light source, 400 W mercury (Hg) vapor lamp was used for the illumination on the suspended photocatalyst of the aqueous reaction mixture kept under constant stirring condition. The distance between the lamp and the photoreactor containing reaction solution was fixed at 8 in. The resulting evolved gases were analyzed by PerkinElmer Clarus 580 GC equipped with 5 Å molecular sieve column, a thermal conductivity detector (TCD) and Argon as the carrier gas. The number of the incident photon was counted using intensity of the incident light, which has been measured using Newport energy meter (model 842-PE). Intensity of the light was measured to be 0.195 W/cm^2 (∼2 sun).

5.2. Binding Kinetics Experiment. Binding kinetics of the phosphine coordinated sensitizers on TiO$_2$ surface was studied by recording the absorption spectra of dye solution at a regular time interval. First, the measured amount of dye was added into 40 mL of MeOH and then it was stirred to make a clear solution. Into the resulting solution, 10 mg of TiO$_2$ was added and subsequently it was kept under stirring condition at room temperature in dark condition. Eventually, at a particular time interval, 3 mL of aliquot was collected, centrifuged at 3500 rpm and then the absorption spectra was recorded.

ASSOCIATED CONTENT

ⓢ Supporting Information

The Supporting Information is available free of charge on the ACS Publications website at DOI: 10.1021/acsami.5b04020.

> Experimental details, electronic absorption and emission intersection spectra of **GS11**, **GS12**, and **GS13**, ^{1}H NMR spectra, and computational details of **GS11**, **-12**, and **-13**. (PDF)

AUTHOR INFORMATION

Corresponding Authors

*E-mail: spsingh@iict.res.in. Tel: +91-40-27191710. Fax: +91-40-27160921.
*E-mail: upal03@gmail.com. Fax: +91-343-2546745. Tel:+91-343-6452136.

Author Contributions

#T.S. and I.M. contributed equally.

Notes

The authors declare no competing financial interest.

REFERENCES

(1) Ruhl, C.; Appleby, P.; Fennema, J.; Naumov, A.; Schaffer, M. Economic Development and the Demand for Enregy: A Histgorical Perspective on the Next 20 Years. *Energy Policy* **2012**, *50*, 109−116.

(2) Fujishima, A.; Honda, K. Electrochemical Photolysis of Water at a Semiconductor Electrode. *Nature* **1972**, *238*, 37−38.

(3) Ni, M.; Leung, M. K. H.; Leung, D. Y. C.; Sumathy, K. A Review and Recent Developments in Photocatalytic Water-Splitting Using TiO$_2$ for Hydrogen Production. *Renewable Sustainable Energy Rev.* **2007**, *11*, 401−425.

(4) Kudo, A.; Miseki, Y. Heterogeneous Photocatalyst Materials for Water Splitting. *Chem. Soc. Rev.* **2009**, *38*, 253−278.

(5) Kim, W.; Tachikawa, T.; Majima, T.; Li, C. H.; Kim, H. J.; Choi, W. Tin-porphyrin Sensitized TiO$_2$ for the Production of H$_2$ under Visible Light. *Energy Environ. Sci.* **2010**, *3*, 1789−179.

(6) Jarosz, P.; Du, P. W.; Schneider, J.; Lee, S. H.; McCamant, D.; Eisenberg, R. Platinum(II) Terpyridyl Acetylide Complexes on Platinized TiO$_2$: Toward the Photogeneration of H$_2$ in Aqueous Media. *Inorg. Chem.* **2009**, *48*, 9653−9663.

(7) Bala, S.; Mondal, I.; Goswami, A.; Pal, U.; Mondal, R. Synthesis, Crystal Structure and Optical Properties of a Naphthylbisimide-Ni Complex: A Framework On TiO$_2$ for Visible Light H$_2$ Production. *Dalton Trans.* **2014**, *43*, 15704−15707.

(8) Takanabe, K.; Kamata, K.; Wang, X.; Antonietti, M.; Kubota, J.; Domen, K. Photocatalytic Hydrogen Evolution on Dye-Sensitized Mesoporous Carbon Nitride Photocatalyst with Magnesium Phthalocyanine. *Phys. Chem. Chem. Phys.* **2010**, *12*, 13020−13025.

(9) Zhang, X.; Veikko, U.; Mao, J.; Cai, P.; Peng, T. Visible-Light-Induced Photocatalytic Hydrogen Production over Binuclear Ru^{II}−Bipyridyl Dye-Sensitized TiO$_2$ Without Noble Metal Loading. *Chem. - Eur. J.* **2012**, *18*, 12103−12111.

(10) Yum, J. H.; Baranoff, E.; Wenger, S.; Nazeeruddin, Md. K.; Gratzel, M. Panchromatic Engineering for Dye-sensitized Solar Cells. *Energy Environ. Sci.* **2011**, *4*, 842−857.

(11) Anderson, P. A.; Strouse, G. F.; Treadway, J. A.; Keene, F. R.; Meyer, T. J. Black MLCT Absorbers. *Inorg. Chem.* **1994**, *33*, 3863−3864.

(12) Kinoshita, T.; Dy, J. T.; Uchida, S.; Kubo, T.; Segawa, H. Wideband Dye-sensitized Solar Cells Employing a phosphine-coordinated Ruthenium Sensitizer. *Nat. Photonics* **2013**, *7*, 535−539.

(13) Kim, J. J.; Choi, H.; Paek, S.; Kim, C.; Lim, K.; Ju, M. J.; Kang, H. S.; Kang, M. S.; Ko, J. A New Class of Cyclometalated Ruthenium Sensitizers of the Type ĈN̂N for Efficient Dye-Sensitized Solar Cells. *Inorg. Chem.* **2011**, *50*, 11340−11347.

(14) Hoffmann, K. J.; Bakken, E.; Samuelsen, E. J.; Carlsen, P. H. Synthesis and Polymerization of 3,3′-Dialkyl-2,2′-Bithiophenes. *Synth. Met.* **2000**, *113*, 39−44.

(15) Huang, C. H.; McClenaghan, N. D.; Kuhn, A.; Hofstraat, J. W.; Bassani, D. M. Enhanced Photovoltaic Response in Hydrogen-Bonded All-Organic Devices. *Org. Lett.* **2005**, 7, 3409−3412.

(16) Turbiez, M.; Frere, P.; Allain, M.; Videlot, C.; Ackermann, J.; Roncali, J. Design of Organic Semiconductors: Tuning the Electronic Properties of π-Conjugated Oligothiophenes with the 3,4-Ethyl-enedioxythiophene (EDOT) Building Block. *Chem. - Eur. J.* **2005**, 11, 3742−3752.

(17) Numata, Y.; Islam, A.; Sodeyama, K.; Chen, Z. H.; Tateyama, Y.; Han, L. Substitution Effects of Ru−Terpyridyl Complexes on Photovoltaic and Carrier Transport Properties in Dye-Sensitized Solar Cells. *J. Mater. Chem. A* **2013**, 1, 11033−11042.

(18) Maestri, M.; Armaroli, N.; Balzani, V.; Constable, E. C.; Thompson, A. M. W. C. Complexes of the Ruthenium(II)-2,2′:6′,2″-terpyridine Family. Effect of Electron-Accepting and -Donating Substituents on the Photophysical and Electrochemical Properties. *Inorg. Chem.* **1995**, 34, 2759−2767.

(19) Chitumalla, R. K.; Gupta, K. S. V.; Malapaka, C.; Fallahpour, R.; Islam, A.; Han, L.; Kotamarthi, B.; Singh, S. P. Thiocyanate-Free Cyclometalated Ruthenium(II) Sensitizers For DSSC: A Combined Experimental and Theoretical Investigation. *Phys. Chem. Chem. Phys.* **2014**, 16, 2630−2640.

(20) Qian, X.; Zhu, Y.-Z.; Song, J.; Gao, X.-P.; Zheng, J.-Y. New Donor-π-Acceptor Type Triazatruxene Derivatives for Highly Efficient Dye-Sensitized Solar Cells. *Org. Lett.* **2013**, 15, 6034−6037.

(21) Wei, L.; Na, Y.; Yang, Y.; Fan, R.; Wang, P.; Li, L. Efficiency of Ruthenium Dye Sensitized Solar Cells Enhanced By 2,6-Bis[1-(Phenylimino)Ethyl]Pyridine as a Co-sensitizer Containing Methyl Substituents On Its Phenyl Rings. *Phys. Chem. Chem. Phys.* **2015**, 17, 1273−1280.

(22) Scanlon, D. O.; Dunnill, C. W.; Buckeridge, J.; Shevlin, S. A.; Logsdail, A. J.; Woodley, S. M.; Catlow, C. R. A.; Powell, M. J.; Palgrave, R. G.; Parkin, I. P.; Watson, G. W.; Keal, T. W.; Sherwood, P.; Walsh, A.; Sokol, A. A. Band Alignment of Rutile and Anatase TiO_2. *Nat. Mater.* **2013**, 12, 798−801.

(23) Kroeze, J. E.; Hirata, N.; Koops, S.; Nazeeruddin, M. K.; Schmidt-Mende, L.; Grätzel, M.; Durrant, J. R. Alkyl Chain Barriers for Kinetic Optimization in Dye-Sensitized Solar Cells. *J. Am. Chem. Soc.* **2006**, 128, 16376−16383.

(24) Herrmann, J. M.; Disdier, J.; Pichat, P. Photoassisted Platinum Deposition on TiO_2 Powder Using Various Platinum Complexes. *J. Phys. Chem.* **1986**, 90, 6028−6034.

(25) Bamwenda, G. R.; Tsubota, S.; Nakamura, T.; Haruta, M. Photoassisted Hydrogen Production from a Water-Ethanol Solution: A Comparison of Activities of $Au.TiO_2$ and $Pt.TiO_2$. *J. Photochem. Photobiol., A* **1995**, 89, 177−189.

(26) Inkson, J. C. Many-Body Effect at Metal-Semiconductor Junctions. II. The Self Energy and Band Structure Distortion. *J. Phys. C: Solid State Phys.* **1973**, 6, 1350.

(27) Hagfeldt, A.; Gratzel, M. Light-Induced Redox Reactions in Nanocrystalline Systems. *Chem. Rev.* **1995**, 95, 49−68.

(28) Kajiwara, T.; Hashimoto, K.; Kawai, T.; Sakata, T. Dynamics of Luminescence from $Ru(bpy)_3cl_2$ Adsorbed on Semiconductor Surfaces. *J. Phys. Chem.* **1982**, 86, 4516−4522.

(29) Peng, T. Y.; Ke, D. N.; Cai, P.; Dai, K.; Ma, L.; Zan, L. Influence of Different Ruthenium(II) Bipyridyl Complex on the Photocatalytic H_2 Evolution Over TiO_2 Nanoparticles with Mesostructures. *J. Power Sources* **2008**, 180, 498−505.

(30) Peng, T. Y.; Dai, K.; Yi, H. B.; Ke, D. N.; Cai, P.; Zan, L. Photosensitization of Different Ruthenium(II) Complex Dyes on TiO_2 for Photocatalytic H_2 Evolution under Visible-Light. *Chem. Phys. Lett.* **2008**, 460, 216−219.

(31) Li, Q.; Jin, Z.; Peng, Z.; Li, Y.; Li, S.; Lu, G. High-Efficient Photocatalytic Hydrogen Evolution on Eosin Y-Sensitized Ti−MCM41 Zeolite under Visible-Light Irradiation. *J. Phys. Chem. C* **2007**, 111, 8237−8241.

(32) Li, Q.; Chen, L.; Lu, G. Visible-Light-Induced Photocatalytic Hydrogen Generation on Dye-Sensitized Multiwalled Carbon Nano-tube/Pt Catalyst. *J. Phys. Chem. C* **2007**, 111, 11494−11499.

(33) Ardo, S.; Meyer, G. J. Photodriven Heterogeneous Charge Transfer with Transition-metal Compounds Anchored to TiO_2 Semiconductor Surfaces. *Chem. Soc. Rev.* **2009**, 38, 115−164.

(34) Lyon, L. A.; Hupp, J. T. Energetics of the Nanocrystalline Titanium Dioxide/Aqueous Solution Interface: Approximate Conduction Band Edge Variations between $H_{0\_} = -10$ and $H\_\_ = +26$. *J. Phys. Chem. B* **1999**, 103, 4623−4628.